PCCP

PAPER

View Article Online
View Journal | View Issue

Cite this: *Phys. Chem. Chem. Phys.*, 2014, **16**, 11597

Warm white light generation from a single phase Dy^{3+} doped $Mg_2Al_4Si_5O_{18}$ phosphor for white UV-LEDs†

Zhipeng Ci,* Qisheng Sun, Shengchun Qin, Mengxing Sun, Xiaojing Jiang, Xudong Zhang and Yuhua Wang*

Received 23rd January 2014,
Accepted 21st March 2014

DOI: 10.1039/c4cp00357h

www.rsc.org/pccp

A series of $Mg_{2-x}Al_4Si_5O_{18}$:xDy^{3+} ($0 \leq x \leq 0.18$) samples were synthesized, for the first time, by a solid state method both in a reducing atmosphere and in air. XRD, diffuse reflectance spectra, excitation spectra, emission spectra, decay times and thermal quenching were used to investigate the structure, photoluminescence, energy transfer and thermal properties. The results show that $Mg_2Al_4Si_5O_{18}$:Dy^{3+} can efficiently absorb UV light and emit violet-blue light in the range of 400 to 500 nm from oxygen vacancies in the host as well as blue light (~480 nm) and yellow light (~576 nm) from the f–f transitions of Dy^{3+}. The emission intensities of the samples obtained under a reducing atmosphere are far superior to those of the samples obtained in air due to an efficient energy transition from oxygen vacancies in the host to Dy^{3+}. An analysis of the thermal quenching shows that the phosphor $Mg_2Al_4Si_5O_{18}$:Dy^{3+} has excellent thermal properties. The emission intensities of typical samples synthesized in a reducing atmosphere and in air at 250 °C are 70% and 81% of their initial intensities at 20 °C, respectively. In addition, the emission colors of all of the samples are located in the white light region and the optimal chromaticity coordinates and Correlated Color Temperature are (x = 0.34, y = 0.33) and 5129 K, respectively. Therefore, these white $Mg_2Al_4Si_5O_{18}$:Dy^{3+} phosphors could serve as promising candidates for white-light UV-LEDs.

1. Introduction

In recent years, with the development of photoelectric technology and materials science, white-light-emitting diodes (WLEDs) have been regarded as a new generation of lighting source after incandescent and energy saving lamps because they are environmentally friendly and energy saving.[1,2] Among the many ways of achieving white light, phosphor-converted (pc) white LEDs have attracted significant attention due to their high efficiency and low cost. There are two methods used to obtain white light emission. One is the combination of a blue LED with a yellow phosphor (YAG:Ce^{3+}), however, this approach leads to a poor color rendering index (Ra = 70–80) and a high Correlated Color Temperature (CCT ≈ 7750 K) because of the lack of a sufficient red component.[3,4] The other method is a combination of an ultra-violet (UV) LED with red–green–blue (RGB) phosphors, which also has some disadvantages such as low luminescent efficiency owing to the strong reabsorption of blue light by the red and green phosphors.[5,6] With respect to these problems, the development of a single-phase white-light emitting phosphor is one of the most effective solutions and has attracted much attention for white LED application.[7]

At present, among the large number of photoluminescence materials available, rare earth doped silicate phosphors are well known for their high efficiency and good chemical stability,[8–16] and have been applied in LED, plasma display panel (PDP) and field emission display (FED) applications. These phosphors include $ZnSiO_4$:Mn^{2+}, Sr_2SiO_4:Eu^{2+} and $M_3MgSi_2O_8$:Eu^{2+}, Mn^{2+} (M = Ca, Sr, Ba), and so on.[17–19] Cordierite silicate $Mg_2Al_4Si_5O_{18}$ (MAO) is an extremely versatile material and has been widely used as a high quality refractory material, in integrated circuit boards as well as a catalyst carrier, a ceramic foam and an aviation material *etc.*, due to its good thermal shock resistance, dielectric properties, fire resistance and mechanical properties.[20,21] In 2003, Thim[22] studied the luminescence properties of Eu^{3+} doped MAO. However, the photoluminescence properties of other rare earth ion doped MAO materials have not been reported. Dy^{3+} is an important dopant that has been widely

Department of Materials Science, School of Physical Science and Technology, Lanzhou University, Lanzhou 730000, China. E-mail: cizhp@lzu.edu.cn; Fax: +86-931-8913554; Tel: +86-931-8912772

† Electronic supplementary information (ESI) available: Fig. S1 shows the PLE and PL spectra of the un-doped MAO samples and the PL spectra of Dy^{3+} doped MAO samples in air and a reducing atmosphere. Fig. S2 presents the Dy 4d XPS spectrum of the MAO:0.18Dy^{3+} sample synthesized in a reducing atmosphere. See DOI: 10.1039/c4cp00357h

used in luminescent materials due to the various transitions between its different energy levels that occur in the UV-Visible and Near Infrared (NIR) region. Many research reports have shown that Dy^{3+} has not only been applied in WLEDs and mercury-free luminescence lamps because of the white emission from its two dominant bands of blue (470–500 nm) and yellow (570–600 nm),[23,24] but it has also been frequently used in light conversion materials by combining it with other rare earth ions like Er^{3+} and Yb^{3+}. In addition, Dy^{3+} usually plays an important role in many long-lasting phosphors, such as $Sr_2Al_2O_4$:Eu^{2+}, Dy^{3+},[25] $Sr_2MgSi_2O_7$:Dy^{3+},[26] and Mg_2SiO_4:Dy^{3+}, Mn^{2+}.[27] Therefore, in order to develop a single phase white emitting phosphor and perform some basic research, in this paper, we have synthesized a series of $Mg_{2-x}Al_4Si_5O_{18}$:xDy^{3+} ($0 \leq x \leq 0.18$) samples using a solid state method in a reducing atmosphere and in air. The photoluminescence, mechanism of energy transfer and thermal properties were then carefully investigated.

2. Experimental

2.1 Materials and synthesis

Stoichiometric amounts of the raw materials, $(MgCO_3)_4 \cdot Mg(OH)_2 \cdot 5H_2O$ (AR), Al_2O_3 (AR), SiO_2 (AR), Dy_2O_3 (AR) and NH_4Cl (AR) (3 wt%, as a flux), were thoroughly mixed in an agate mortar with ethanol. Firstly, the mixture was heated up to 600 °C for 6 h, then the mixture was reground and further fired at 1400 °C for 10 h in an alumina crucible under air and N_2–H_2 (8%) atmospheres in a horizontal tube furnace, and then slowly cooled to room temperature. Finally, two samples, one synthesized in air, the other in a reducing atmosphere were obtained.

2.2 Measurements and characterization

The crystal structures of the synthesized samples were identified using a Rigaku D/Max-2400 X-ray diffractometer with Ni filtered Cu Kα radiation (XRD). Diffuse reflectance spectra were obtained with a UV/visible spectrophotometer (Perkin-Elmer Lambda 950) using $BaSO_4$ as a reference in the range of 240–700 nm. The photoluminescence (PL) and photoluminescence excitation (PLE) spectra of the samples were measured using an FLS-920T fluorescence spectrophotometer equipped with a 450 W Xe light source, a Xe flash lamp and a ns pulsed hydrogen lamp. The quantum efficiency was measured using a Fluorlog-3 spectrofluorometer equipped with a 450 W Xe lamp (Horiba Jobin Yvon). All of the measurements were performed at room temperature. Thermal quenching was tested using a heating apparatus (TAP-02) in combination with PL equipment.

3. Results and discussion

3.1 Crystal structure of MAO

Fig. 1(a) shows the XRD patterns of the MAO:xDy^{3+} ($0 \leq x \leq 0.18$) samples synthesized in a reducing atmosphere and in air. All of the observed diffraction peaks are well indexed to the

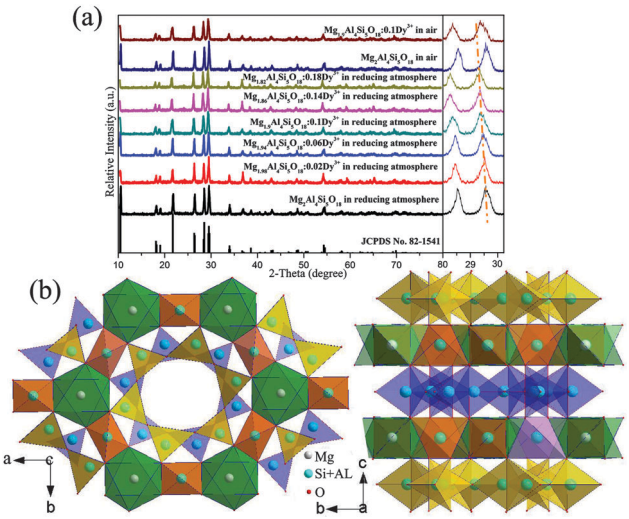

Fig. 1 (a) The XRD patterns of the MAO:xDy^{3+} ($0 \leq x \leq 0.18$) samples synthesized in a reducing atmosphere and in air. (b) A structure diagram of MAO.

phases of $Mg_2Al_4Si_5O_{18}$ (JCPDS No. 82-1541) and no second phase is observed, indicating that the doping ions do not cause any significant changes in the host. Fig. 1(b) shows a structure diagram of MAO. Cordierite MAO, which has an ideal composition of $Mg_2Al_4Si_5O_{18}$, is a Mg aluminosilicate. It has an orthorhombic structure (space group *Cccm*) with four molecules in each unit cell. In the structure, there is only one Mg^{2+} site coordinated by 6 O^{2-}. Si^{4+} and Al^{3+} are both surrounded by 4 O^{2-} and form a tetrahedron. Similar to those of beryllium, the Si/Al-tetrahedra form Si_6O_{18}-type 6-membered-rings with one Al substituted for one Si in the ring. The Si atoms in the rings are bonded to two oxygen atoms in the ring and to two oxygen atoms in layers above and below. There is no direct bonding between rings, but they are linked by Mg in the octahedra and by Al in the tetrahedra above and below.[28] When doping ions are introduced into the MAO host, in principle, they could be incorporated into any one of the three cation sites,[29,30] *i.e.*, Mg^{2+} (ionic radius: 0.72 Å), Al^{3+} (0.39 Å) and Si^{4+} (0.26 Å) (the ionic radii are from ref. 31 and Table 1). The effective ionic radius of Dy^{3+} is 0.91 Å (for a sixfold coordinated Dy^{3+} ion. Data on fourfold coordination are currently not available).[31] A comparison of the ionic radii mismatch, however, points to Mg^{2+}-sites as the most probable host for Dy^{3+}. In addition, according to the reports of Sai[32] and Tang,[33] the Mg^{2+} (0.72 Å) in MAO can be replaced by bigger ions such as Ca^{2+} (1.00 Å),[31] Sr^{2+} (1.18 Å)[31] and Ba^{2+} (1.35 Å)[31] to form a solid solution. Therefore, it is possible that Dy^{3+} is introduced into the MAO host and, as

Table 1 Relative difference in the ionic radii (dr(%) = 100 × [R_m(CN) − R_d(CN)]/R_m(CN)) between the matrix cations and the dopant, Dy^{3+}

Ions	Radius/Å	CN	dr(%)
Dy^{3+}	0.91	6	0
Mg^{2+}	0.72	6	−26.39
Al^{3+}	0.39	4	−133.33
Si^{4+}	0.26	4	−250

shown in Fig. 1(a), it is clearly observed that the XRD peaks slightly shift towards smaller angles due to the bigger radius of Dy^{3+} *versus* Mg^{2+}.

3.2 Photoluminescence properties analysis

In Fig. 2(a), the dotted lines represent the diffuse reflectance spectra (DFS) of MAO and MAO:0.1Dy^{3+} synthesized in air. Both samples demonstrate a remarkable drop in the ultraviolet (UV) range from 200 to 380 nm due to the absorption of the host. Compared with pure MAO, some new sharp drops at 347, 364, 386, 425 and 453 nm in the DFS of MAO:0.1Dy^{3+} are observed and can be ascribed to the characteristic transitions $^6H_{15/2} \rightarrow {}^6P_{7/2}$, $^6P_{5/2}$, $^4M_{21/2}$, $^4G_{11/2}$ and $^4I_{15/2}$ of Dy^{3+}, respectively.[34] Photoluminescence spectra of MAO show the MAO sample synthesized in air can be excited by UV light from 250 to 380 nm and emit blue light from 400 to 500 nm. In order to find the reasons for this self-illumination, another MAO sample was synthesized in a reducing atmosphere. It is clearly observed that the shapes of the PLE and PL spectra for both samples are very similar, but the emission intensity of the MAO synthesized in a reducing atmosphere is far greater than that of the sample synthesized in air. This implies that the broad blue emission band could mainly arise from oxygen vacancies in the MAO host. Detailed reasoning is shown in ESI,† Fig. S1 and S2. The PLE spectra of MAO:0.1Dy^{3+} synthesized in a reducing atmosphere and in air are also presented in Fig. 2(a). There is an obvious spectral overlap between the PL of MAO and PLE of MAO:0.1Dy^{3+}, which suggests that an energy transfer between Dy^{3+} and the oxygen vacancies in the MAO host could occur. Fig. 2(b) and (c) show the PLE (λ_{em} = 576 nm) and PL (λ_{ex} = 350 nm) spectra of MAO:$x$$Dy^{3+}$ synthesized in a reducing atmosphere and in air. The sharp excitation peaks from 350 to 470 nm can be attributed to the intra-4f forbidden transitions from the ground level $^6H_{15/2}$ to higher energy levels of Dy^{3+},[35] which is consistent with the DRS of MAO:Dy^{3+} in Fig. 2(a). An ideal phosphor for UV-LEDs should have strong absorption from about 350 to 410 nm (the emission wavelengths of UV-LED chips).[36,37] Notably, the excitation spectra of MAO:$x$$Dy^{3+}$ exhibit strong absorption from around 350 to 410 nm, indicating they could be candidates for yellow or white phosphors in UV-LEDs. The emission spectra mainly consist of a broad band from 400 to 500 nm and three characteristic emission peaks located at 482, 576 and 665 nm, which can be attributed to emission from the oxygen vacancies in the MAO host and the $^4F_{9/2}$–$^6H_{15/2}$, $^4F_{9/2}$–$^6H_{13/2}$ and $^4F_{9/2}$–$^6H_{11/2}$ transitions of Dy^{3+}, respectively. As the amount of Dy^{3+} increases, the emission intensities for Dy^{3+} gradually increase, but those related to oxygen vacancies in the MAO host gradually decrease, which also supports the idea that there is an energy transfer between Dy^{3+} and the oxygen vacancies in the MAO host. For the samples synthesized in a reducing atmosphere and air, the optimal Dy^{3+} amount is x = 0.1. This critical concentration (5%) is referred to as the ''quenching concentration''. In general, a concentration quenching effect is caused by a non-radiative energy transfer process between the neighboring Dy^{3+} ions when the Dy^{3+} concentration reaches a critical value. Therefore, the quenching concentration can be more accurately determined using changes in the decay times of Dy^{3+}. Fig. 2(d) shows

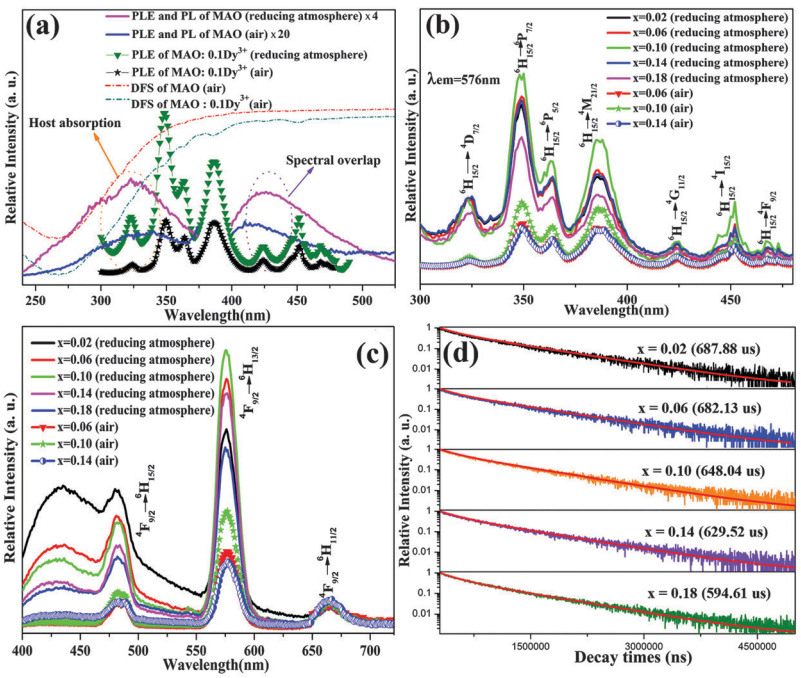

Fig. 2 (a) The PLE (λ_{em} = 425 nm) and PL (λ_{ex} = 325 nm) spectra of MAO, the PLE (λ_{em} = 576 nm) spectra of MAO:0.1Dy^{3+} synthesized in a reducing atmosphere and air and the DFS of MAO and MAO:0.1Dy^{3+} obtained in air; (b) and (c) the PLE (λ_{em} = 576 nm) and PL (λ_{ex} = 350 nm) spectra of MAO:$x$$Dy^{3+}$ synthesized in a reducing atmosphere and air; (d) decay curves of MAO:$x$$Dy^{3+}$ with different Dy^{3+} concentrations (λ_{ex} = 386 nm, λ_{em} = 576 nm) synthesized in a reducing atmosphere.

how the decay time depends on the Dy^{3+} content when excited at 386 nm and with the emission monitored at 576 nm. The decay times (τ) were calculated to be 687.88, 682.13, 648.04, 629.52 and 594.61 μs as the Dy^{3+} content increased from 1% to 9%. It can be clearly observed that the decay times gradually decrease and when the Dy^{3+} content x reaches 5%, the decay time sharply declines, which might be an indication that an energy transfer between Dy^{3+} ions is occurring. Thus, the quenching concentration was further confirmed to be 5% by the changes in the decay times. The quantum efficiency of the optimum MAO:0.1Dy^{3+} sample synthesized in a reducing atmosphere is 18.1%. The critical distance R_c of energy transfer between Dy^{3+} ions is an important parameter for evaluating the photoluminescence properties and could be calculated using the critical concentration of the activator ion as follows:[38,39]

$$R_c \approx 2\left(\frac{3V}{4\pi x_c N}\right)^{1/3}$$

where V is the volume of the unit cell, x_c is the critical concentration of the activator ion, and N is the number of cations per unit cell. For the MAO host, $N = 8$, $x_c = 0.05$, and $V = 1550.48$ Å^3, so the R_c value was calculated to be about 19.49 Å.

To further understand the process of energy transfer, the decay times of MAO:$x$$Dy^{3+}$ with different Dy^{3+} concentrations excited at 325 nm and monitored at 425 nm were measured and are depicted in Fig. 3(a). The corresponding luminescent decay curves can be fitted using a multi-exponential model. The average decay times were calculated and are listed in Fig. 3(a). The PL decay time of MAO decreased from 8.13 to 5.39 ns when the Dy^{3+} concentration was increased to 9%. The energy transfer efficiency η is defined as the ratio between the number of depopulation events that result in energy transfer from donor to acceptor and the total population of the excited states in the donor. It can be calculated from the ratio of the decay times of the excited state(s) of the donor in the presence of the acceptor by comparing to a specimen that contains only the donor species.[40,41] Therefore, the energy transfer efficiency η_{MAO-Dy} can be obtained by:

$$\eta = 1 - \frac{\tau_S}{\tau_{S0}}$$

where τ_{S0} is the decay time of the host MAO in the absence of Dy^{3+} and τ_S is the decay time of the host MAO in the presence of Dy^{3+}. The decay times were used for the calculation and the results are presented in Fig. 3(b). With an increase of Dy^{3+} concentration, the energy transfer efficiency η_{MAO-Dy} increases from 9% to 33%. Fig. 3(c) shows the Commission International de L' Eclairage (CIE) chromaticity coordinates of the samples calculated based on their corresponding PL spectra. The emission colors of all of the samples are located in the white light region with the optimum chromaticity coordinates and CCT being (x = 0.34, y = 0.33) and 5129 K, which are very close to standard white (x = 0.33, y = 0.33). The full details of the chromaticity coordinates and CCT are listed in Table 2.

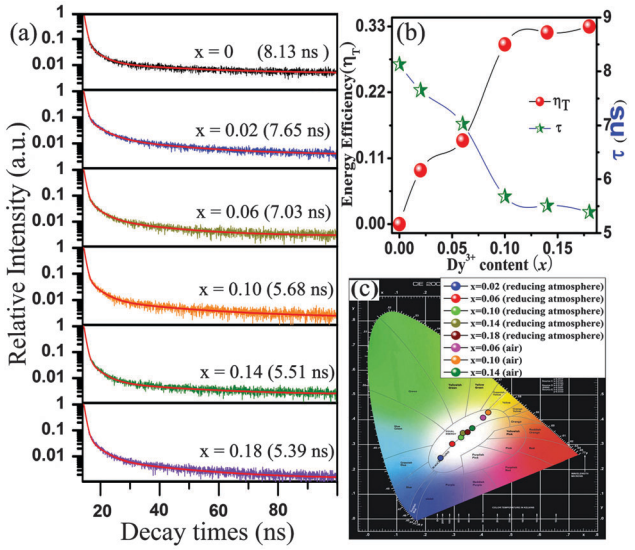

Fig. 3 (a) Decay curves for MAO:$x$$Dy^{3+}$ with different Dy^{3+} concentrations (λ_{ex} = 325 nm, λ_{em} = 425 nm); (b) the relationship between the decay time and the energy transfer efficiency with increasing Dy^{3+} content; (c) the CIE chromaticity coordinates of the MAO:$x$$Dy^{3+}$ samples synthesized in a reducing atmosphere and air.

3.3 Thermal properties analysis

In general, in the process of a phosphor's application, the emission intensities of the phosphor are reduced by thermal phonon-assisted relaxation, through the crossing point between the excited and the ground states.[42–45] Therefore, the thermal quenching characteristics are of great significance for phosphors. The temperature dependent luminescence properties for MAO:0.1Dy^{3+} synthesized in a reducing atmosphere and air were tracked in the temperature ranged from 20 to 250 °C, and the results are shown in Fig. 4(a) and (b). With increasing temperature, the emission intensities of all of the samples gradually decline. The emission intensities of MAO:0.1Dy^{3+} synthesized in a reducing atmosphere and air are 70% and 81% of their initial intensities at 20 °C, respectively, which indicates that the MAO:0.1Dy^{3+} phosphors have excellent thermal stabilities. Fig. 4(c) shows that the normalized emission intensities of MAO:0.1Dy^{3+} synthesized in a reducing atmosphere are obviously above those of the samples synthesized in air below 150 °C and then rapidly decline when the temperature exceeds

Table 2 Detailed data for the emission colors, CIE and CCT of the MAO:$x$$Dy^{3+}$ samples synthesized in a reducing atmosphere and air as well as blue chips + YAG

Samples composition	Color	CIE		CCT (K)
		x	y	
MAO:0.02Dy^{3+}(reducing)	Blue white	0.26	0.25	—
MAO:0.06Dy^{3+}(reducing)	White	0.31	0.30	6936
MAO:0.10Dy^{3+}(reducing)	White	0.34	0.33	5129
MAO:0.14Dy^{3+}(reducing)	White	0.34	0.35	5192
MAO:0.18Dy^{3+}(reducing)	White	0.35	0.35	4798
MAO:0.06Dy^{3+}(air)	Warm white	0.41	0.41	3510
MAO:0.10Dy^{3+}(air)	Warm white	0.42	0.43	3456
MAO:0.14Dy^{3+}(air)	Warm white	0.36	0.36	4493
blue chips + YAG	White	0.29	0.30	5610

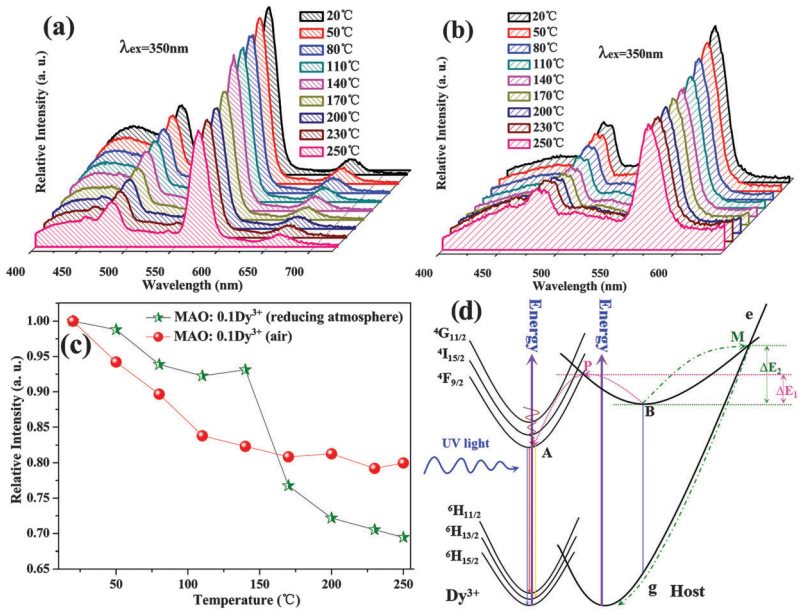

Fig. 4 The PL spectra of MAO:0.1Dy^{3+} synthesized in a reducing atmosphere (a) and air (b) at various temperatures. (c) The dependence of the normalized PL intensities on temperature for the phosphors. (d) The configurational coordinate diagram of the ground and excited states of Dy^{3+} and the oxygen vacancies in the MAO host.

150 °C. This phenomenon could be explained using the configurational coordinate diagram shown in Fig. 4(d). The curves for ^6H_j (j = 11/2, 13/2 and 15/2) and $^4G_{11/2}$, and $^4I_{15/2}$ and $^4F_{9/2}$ represent the ground and excited states of Dy^{3+}, respectively. The curves g and e represent the ground and excited states of the oxygen vacancies in MAO host, respectively. Points A and B are the lowest positions of $^4F_{9/2}$ and e curves, respectively. Point M is the crossing point of curves e and g, while point P is the crossing point of curves e and the excited states of Dy^{3+}. In order to simplify the discussion, only one crossing point of e and the excited states of Dy^{3+} (P) are marked. At room temperature, the electrons in ^6H_j and g are firstly excited to their excited states under excitation at 350 nm. For the excited states of Dy^{3+}, most of the electrons return to their ground states *via* a radiative transition. However, for excited state e, in addition to the radiative transition, a percentage of the electrons in e are very likely to be able to overcome the energy barrier ΔE_1 and transfer their energy to ^6H_j due to electron–phonon coupling and, thereby, the emission intensity of Dy^{3+} is enhanced. With an increase in temperature, more electrons in excited state e can overcome energy barrier ΔE_1 due to stronger electron–phonon coupling and transfer to the excited states of Dy^{3+} from the crossing point P, which consequently slows down the decline of the emission intensity of Dy^{3+}. However, with a further increase of temperature, the electrons in excited state e would also probably overcome energy barrier ΔE_2 under stronger phonon vibration and directly tunnel to the ground state g, which results in the rapid decrease observed in the energy transfer efficiency between the oxygen vacancies in the MAO host and Dy^{3+}. This further the sharp decline in the emission intensity of Dy^{3+} when the temperature is above about 150 °C. Meanwhile, from Fig. 2(c), the emission intensity of Dy^{3+} in MAO:Dy^{3+} synthesized in a reducing atmosphere is far above that in the sample synthesized in air. It indicates that the emission intensity of Dy^{3+} is seriously influenced by oxygen vacancies in the MAO host. Therefore, with the rapid decrease of the energy transfer efficiency between the oxygen vacancies and Dy^{3+}, the thermal properties of MAO:Dy^{3+} synthesized in the reducing atmosphere becomes worse than that of the sample synthesized in air in the normalized intensities of the temperature-dependent PL spectra (see in Fig. 4(c)).

4. Conclusions

In conclusion, a series of novel single phase white-emitting MAO:$x$$Dy^{3+}$ ($0 \leq x \leq 0.18$) phosphors have been synthesized using a solid state method in a reducing atmosphere and air. The luminescence properties, thermal stability as well as the mechanism of energy transfer from oxygen vacancies in the MAO host to Dy^{3+} have been carefully investigated for the first time. Upon 350 nm excitation, the phosphor exhibits a blue broad band emission centered at 425 nm due to emission from the oxygen vacancies and two sharp peaks at 480 and 576 nm, which can be ascribed to the f–f transitions of Dy^{3+}. As energy transfer occurs from the oxygen vacancies to Dy^{3+}, the emission intensities of MAO:Dy^{3+} obtained in the reducing atmosphere are far stronger than those of the samples obtain in air. More importantly, a wavelength-tunable white light can be achieved with optimum CIE chromaticity coordinates (x = 0.34, y = 0.33) and a CCT of 5129 K. The temperature-dependent PL spectra shows that MAO:0.1 Dy^{3+} has excellent thermal properties. The emission intensities of MAO:0.1Dy^{3+} synthesized in a reducing atmosphere and air at 250 °C are 70% and 81% of their initial intensities at 20 °C, respectively. In addition, the emission

intensities of MAO:0.1Dy^{3+} samples obtained in a reducing atmosphere are superior to those of the samples obtained in air when the temperature is below 150 °C, but the opposite case is true when the temperature exceeds 150 °C. Using a configurational coordinate diagram, this phenomenon could be reasonably explained. All of the results indicate that MAO:Dy^{3+} could potentially serve as a single phase white-emitting phosphor for white-light UV-LEDs.

Acknowledgements

This work has been supported by the Young Scientists Fund of the National Natural Science Foundation of China (Grant No. 51302121) and the Nature Science Foundation of Gansu Province (Grant Number: 1107RJZA206).

Notes and references

1 P. F. Smet, K. Korthout, J. E. Haecke and D. Poelman, *Mater. Sci. Eng., B*, 2007, **146**, 264.
2 M. M. Haque, H. I. Lee and D. K. Kim, *J. Alloys Compd.*, 2009, **481**, 792.
3 K. P. Joung, H. K. Chang, H. P. Seung, D. P. Hee and Y. C. Se, *Appl. Phys. Lett.*, 2004, **84**, 1647.
4 Y. Hu, W. Zhuang, H. Ye, D. Wang, S. Zhang and X. Huang, *J. Alloys Compd.*, 2005, **390**, 226.
5 M. A. Lim, J. K. Park, C. H. Kim, H. D. Park and M. W. Han, *J. Mater. Sci. Lett.*, 2003, **22**, 1351.
6 J. Y. Kuang and Y. L. Liu, *Chem. Lett.*, 2005, **34**, 59.
7 J. S. Kim, P. E. Jeon, J. C. Choi, H. L. Park, S. I. Mno and G. C. KIM, *Appl. Phys. Lett.*, 2004, **84**, 2931.
8 X. Yang, S. T. Tan, X. Yu, H. V. Demir and X. W. Sun, *ACS Appl. Mater. Interfaces*, 2011, **3**, 4431.
9 B. Wang, L. Sun and H. Ju, *Solid State Commun.*, 2010, **150**, 146.
10 W. J. Yang, L. Luo, T. M. Chen and N. S. Wang, *Chem. Mater.*, 2005, **17**, 3883.
11 D. S. Jo, Y. Y. Luo, K. Senthil, K. Toda, B. S. Kim, T. Masaki and D. H. Yoon, *Opt. Mater.*, 2011, **34**, 696.
12 X. Yu, X. Xu, P. Yang, Z. Yang, Z. Song, D. Zhou, Z. Yin, Q. Jiao and J. Qiu, *Mater. Res. Bull.*, 2012, **47**, 117.
13 M. D. Que, Z. P. Ci, Y. H. Wang, G. Zhu, S. Y. Xin, Y. R. Shi and Q. Wang, *CrystEngComm*, 2013, **15**, 6389.
14 W. Lu, Z. Hao, X. Zhang, Y. Luo, X. Wang and J. Zhang, *Inorg. Chem.*, 2011, **50**, 7846.
15 J. Y. Han, W. B. Im, D. Kim, S. H. Cheong, G. Lee and D. Y. Jeon, *J. Mater. Chem.*, 2012, **22**, 5374.
16 Z. P. Ci, M. D. Que, Y. R. Shi, G. Zhu and Y. H. Wang, *Inorg. Chem.*, 2014, **53**, 2195.
17 L. Juan, D. P. Fu, Z. Rui, H. L. Yan and J. S. Hyo, *J. Mater. Chem.*, 2011, **21**, 16398.
18 H. L. Jee and J. K. Young, *Mater. Sci. Eng., B*, 2008, **146**, 99.
19 O. Emel and K. Semra, *Ceram. Int.*, 2010, **36**, 1033.
20 M. A. Camerucci, G. Urretavizcaya, M. S. Castro and A. L. Cavalieri, *J. Eur. Ceram. Soc.*, 2001, **21**, 2917.
21 K. N. Milan and C. Minati, *J. Eur. Ceram. Soc.*, 2004, **24**, 3499.
22 G. P. Thim, H. F. Brito, S. A. Silva, M. A. Olivelra and M. C. Felin, *J. Solid State Chem.*, 2003, **171**, 375.
23 Y. Kamiyanagi, M. Kitaura and M. Kaneyoshi, *J. Lumin.*, 2007, **122**, 509.
24 B. Liu, L. J. Kong and C. S. Shi, *J. Lumin.*, 2007, **122**, 121.
25 L. Lin, M. Yin, C. S. Shi and W. P. Zhang, *J. Alloys Compd.*, 2008, **455**, 327.
26 K. N. Shinde, S. J. Dhoble and K. Animesh, *J. Lumin.*, 2011, **13**, 1931.
27 R. Zhang and X. Wang, *J. Alloys Compd.*, 2011, **509**, 1197.
28 B. E. Douglas and S. M. Ho, *Structure and Chemistry of Crystalline Solids*, Springer, 2006, p. 260.
29 G. J. Gao and L. Wondraczek, *Opt. Mater. Express*, 2014, **4**, 476.
30 G. J. Gao, S. Reibstein, M. Y. Peng and L. Wondraczek, *J. Mater. Chem.*, 2011, **21**, 3156.
31 R. D. Shannon, *Acta Crystallogr., Sect. A: Cryst. Phys., Diffr., Theor. Gen. Crystallogr.*, 1976, **32**, 751.
32 S. V. S. Sai, S. Vepa and M. U. Arun, *J. Am. Ceram. Soc.*, 1993, **76**, 1873.
33 F. H. Tang, J. D. Zhuang, F. Fei and Q. Liu, *Chin. J. Chem. Phys.*, 2012, **25**, 345.
34 J. L. Cai, R. Y. Li, C. J. Zhao, S. L. Tie, X. Wan and J. Y. Shen, *Opt. Mater.*, 2012, **34**, 1112.
35 I. Omkaram and S. Buddhudu, *Opt. Mater.*, 2009, **32**, 8.
36 F. P. Du, Y. Nakai, T. J. Tsuboi, Y. L. Huang and H. J. Seo, *J. Mater. Chem.*, 2011, **21**, 4669.
37 C. H. Huang, T. M. Chen, W. R. Liu, Y. C. Chiu, Y. T. Yeh and S. M. Jang, *ACS Appl. Mater. Interfaces*, 2010, **2**, 259.
38 G. Blasse, *Philips Res. Rep.*, 1969, **24**, 131–144.
39 X. M. Liu, C. K. Lin and J. Lin, *Appl. Phys. Lett.*, 2007, **90**, 081904.
40 G. J. Gao and L. Wondraczek, *Opt. Mater. Express*, 2013, **3**, 633.
41 G. J. Gao and L. Wondraczek, *J. Mater. Chem. A*, 2013, **1**, 1952.
42 Y. S. Tang, S. F. Hu, C. C. Lin, N. C. Bagkar and R. S. Liu, *Appl. Phys. Lett.*, 2007, **90**, 151108.
43 V. Bachmann, C. Ronda, O. Oeckler, W. Schnick and A. Meijerink, *Chem. Mater.*, 2009, **21**, 316.
44 H. Luo, J. Liu, X. Zheng, L. Han, K. Ren and X. Yu, *J. Mater. Chem.*, 2012, **22**, 15887.
45 R. J. Xie, N. Hirosaki, T. Suehiro, F. F. Xu and M. Mitomo, *Chem. Mater.*, 2006, **18**, 5578.

